# INELASTIC ANALYSIS OF A MULTICAVITY PCRV UNDER INTERNAL PRESSURE

T. TAKEDA, T. YAMAGUCHI, K. IMOTO

*Structural Engineering Laboratory,*
*Technical Research Institute, Ohbayashi-Gumi, Ltd., Kiyose-shi, Tokyo, Japan*

## SUMMARY

This paper presents two different methods of inelastic analysis, the two- and the three-dimensional finite element technique, and discusses the capabilities of the both methods of analysis to a multicavity prestressed concrete reactor vessel (a multicavity PCRV).

The paper is composed of three parts.

The first part briefly reviews some of the basic concepts of the finite element method in regard to the inelastic analysis of two-dimensional ring element, three-dimensional solid and some other elements, which are at disposal for idealization of various structural components in a PCRV.

The second part presents mainly an idealization of analytical model for a multicavity PCRV. The multicavity PCRV under investigation is a thick-walled cylindrical concrete structure with six additional cavities located in the barrel wall, the both ends of which are bounded by two flat slabs. Moreover, it is mounted on a star-shaped pedestal monolithically cast with the PCRV bottom slab and the base mat, and in the top head slab, a number of refueling penetrations are provided.

On the two-dimensional analysis, a series of simplifications are made in the analytical model. In these simplifications, the multicavity PCRV is replaced by an axisymmetric structure with a solid wall and a solid plate, which is geometrically similar to the original structure but has modified values of the elastic constants. In addition, the local pressure applied at the additional cavities is replaced by an axisymmetric equivalent load. In a similar manner, local reinforcing steel provided in the original structure are replaced by axisymmetric members.

In the three-dimensional analysis, the analytical model is idealized in a portion of multicavity PCRV in consideration of the geometrical symmetry.

The third part illustrates the capabilities of the both methods of inelastic analysis for the multicavity PCRV, using a number of examples with an experimental study of a 1/20th scale PCRV model.

## 1. Introduction

This report presents two different procedures of inelastic analysis for a multicavity prestressed concrete reactor vessel (PCRV), and discusses capabilities of both analytical procedures, comparing these calculated results with test results of a 1/20th scale PCRV model under hydraulic internal pressure.

One of procedures is a two-dimensional analysis employing the two-dimensional finite element technique with ring elements. This procedure uses a modified axisymmetrical model, with a concept of effective elastic constants, representative of multicavity PCRV structures which, by nature of its geometrical configuration, requires a three-dimensional analysis to estimate exactly the elastic as well as the inelastic response of the structure. Basic concept of effective elastic constants has already been mentioned in the analytical procedure of perforated plate problems by T. Slot, W.J. O'Donnel, et al. [1]~[3].

The other procedure of inelastic analysis employs the three-dimensional finite element technique with solid elements.

In these analyses for a concrete composite structure, several kinds of finite element models representative of various structural components such as concrete, steel liners, tendons and bonded reinforcing bars, etc., are taken into account. Considerations of concrete cracks, concrete compressive yield and steel yield are taken in the two-dimensional analysis, while, in the three-dimensional analysis, only consideration of concrete cracks is taken. It has been examined in our single cavity PCRV model test [4] that fundamental assumptions used for the two-dimensional analysis are reliable.

## 2. Basic Methods of the Inelastic Finite Element Analysis

Three kinds of computer programs have been developed for inelastic analysis of a PCRV by the finite element method. Those consist of the two computer programs for two-dimensional problems of a plane or an axisymmetrical structure and the one for three-dimensional problems.

Some basic assumptions, idealization of finite element models and numerical solution methods used for these programs are as follows:

### 2.1 Concrete

Stress-strain relationship The uniaxial concrete stress-strain relationship considered in this investigation is shown in Fig.-1 and it is assumed to be identical with equivalent stress-equivalent strain relationship under multi-axial stress state. Concrete in tension is considered to be brittle material, while, in compression to be strain hardening material up to the critical strain when concrete reaches the strain at crushing, and after crushing to be strain softening material.

Concrete is also assumed to be isotropic material prior to cracking or yielding. The elastic-plastic model by the plastic theory of Yamada [5] is applied in plastic region, that is, plastic stress-strain matrix [DP] is given as following form;

$$[D^p] = [D^e] - \frac{[D^e]\left\{\frac{\partial f}{\partial \sigma}\right\}\left\{\frac{\partial f}{\partial \sigma}\right\}^T[D^e]}{g + \left\{\frac{\partial f}{\partial \sigma}\right\}^T[D^e]\left\{\frac{\partial f}{\partial \sigma}\right\}} \qquad (1)$$

where g is a strain hardening factor, $[D^e]$ is an elastic stress-strain matrix of Hooke's law, and f is scalar function of stresses by Prager-Drucker's yield criterion and can be written as follows;

$$f = \alpha J_1 + \sqrt{J_2} \qquad (2)$$

in which $J_1 = \sigma_x + \sigma_y + \sigma_z$ : first stress invariant

$$J_2 = (\sigma_x^2 + \sigma_y^2 + \sigma_z^2 - \sigma_x\sigma_y - \sigma_y\sigma_z - \sigma_z\sigma_x + 3\tau_{xy}^2 + 3\tau_{yz}^2 + 3\tau_{zx}^2)/3 \qquad (3)$$

: second stress invariant, and $\alpha$ is a constant defined by the material used.

Each yielding element must be examined whether strain reversal causes or not by means of examinations of scalar function increment (df); i.e., if $df \geq 0$ the element remains in plastic state, and if $df < 0$ its stiffness should be returned back to elastic state due to strain reversal.

Failure of concrete  Cracking: If the maximum principal stress is greater than the tensile strength of concrete, cracking occurs along a plane normal to the principal stress direction. When cracking occurs, unbalanced nodal forces equivalent to the maximum principal stress are calculated and redistributed to the other portions of the structure. After cracking the concrete is considered to be un-isotropic.

Crushing: When equivalent strain is reached the critical strain, crushing occurs. Hereafter the behavior of the concrete is assumed to be softening material. This means herein that with the growth of the equivalent strain the stresses are assumed to degrade as shown in Fig.-1.

## 2.2 Steel

The uniaxial steel stress-strain relationship is considered to be bi-linear as shown in Fig.-1. The steel reinforcement is assumed to transmit only axial force. The effects of dowel action in reinforcements and bond slip between reinforcement and concrete are not considered. The Von Mises yield criterion is used for steel liners and strain reversal in yielding element is examined by the proportional constant of Reuss.

## 2.3 Finite Element Idealization

In two different idealized analytical models for plane stress analysis, constant strain triangular plane elements for concrete, and constant strain bar elements for reinforcing bars or liners are adopted, respectively.

In axisymmetrical problem, constant strain triangular linkage elements for concrete, membrane ring elements for liners, constant strain bar elements for prestressing tendons or reinforcing bars are used, respectively. As shown in Fig.-3, the multicavity PCRV is devided into 708 triangular elements, 67 membrane elements, 267 bar elements and 97 ring-

bar elements accompanied with 454 nodes.

In three-dimensional problem, twenty-node arbitrary hexahedral elements for concrete, eight-node curved quadrilateral membrane elements for liners, and three-node arbitrary bar elements for prestressing tendons or reinforcing bars are used, respectively. As shown in Fig.-4, the same PCRV is devided into 139 hexahedral elements, 79 membrane elements and 340 bar elements accompanied with 990 nodes.

In this case, Gaussian integration is used to obtain each element stiffness. Therefore all stresses and strains are evaluated at the Gaussian integration points.

Here, 2-2-2 integration point mesh for hexahedral elements, 3-3 integration point mesh for membrane and 2 integration point for bar elements are used.

Computations are carried out by tangent stiffness method for two-dimensional and axisymmetrical problems, and secant stiffness method for three dimensional problem.

For every increment of load, iteration are repeated until convergence is attained.

The Frontal Solution program written by Iron [6] is used for solution process of linear equations.

## 3. Idealization of Analytical Model

The multicavity PCRV under investigation is a thick walled concrete composite structure. It is a right circular cylinder with flat end slabs supported on a star-shaped concrete pedestal consisting of six wall-legs, which is monolithically cast with the base mat and the PCRV bottom head slab. Six additional cavities (S/G cavities) located in the barrel wall of the PCRV are connected independently to a central core cavity by two circular cross ducts. These cavities and cross ducts are steel lined, providing a leak-tight membrane, and a number of refueling penetrations located in the top head slab are also steel lined.

Wires wound around the external circumference of the barrel and vertical unbonded tendons provide the force required for the entire structure to maintain an essentially elastic response in service condition. Bonded reinforcing bars are placed at many locations for control of concrete cracks.

Geometrical dimensions of the test model used for internal pressure test are shown in Fig.-2.

### 3.1 Analytical Model Idealized into Axisymmetrical Structure

Stiffnesses of the barrel wall with S/G cavities (multicavity barrel) and the top head slab with numerous penetrations (perforated plate) depend on the configuration effects of the holes located in themselves. Therefore, these configuration effects on the evaluation of equivalent stiffnesses shall be taken into account.

The analytical model of the test model, as shown in Fig.-2, is idealized into an axisymmetrical structure consisting of a solid barrel and a solid plate with effective elastic constants.

The methods of evaluation of the equivalent stiffness and local loads (S/G cavity pressure) used for this analytical model, as shown in Fig.-3, are as follows:

(1) Evaluation of the Stiffness for the Perforated Plate with a Triangular Penetration Pattern

The effective elastic constants depend on the reinforcing effect of penetration liners

as well as the configuration effect of holes in the perforated plate. In this report, the effective elastic constants are obtained as shown in Figs.-4.1, 4.2.

$$\xi = t/r_p \quad , \quad \eta = h/p \quad , \quad \Phi = E_s/E_c$$

where, $t$ = plate thickness of penetration liner

$r_p$ = radius of holes in the perforated plate

$h$ = nominal width of ligament at the minimum cross section

$p$ = nominal distance between hole centerlines (pitch)

$E_s$ = Young's modulus of steel

$E_c$ = Young's modulus of concrete

These effective elastic constants are determined so that gross deformations in the perforated material and the equivalent solid material be the same under both plane stress and plane strain conditions, respectively.

The effective Young's modulus $E^*$ and the effective Poisson's ratio $\nu^*$ of the top head slab with steel stand pipes ($\xi = 0.132$, $\eta = 0.474$ and $\Phi = 6.7$) in the 1/20th PCRV model are $E^* \approx E_c$ and $\nu^* \approx \nu_c$, respectively.

(2) Evaluation of the Equivalent Stiffness of the Multicavity Barrel

Using solutions of elastic theory to the two different plane models as shown in Fig.-5, the effective elastic constants of the multicavity barrel are determined from the requirement that the radial displacements at the outer and inner surface on the centerline of a S/G cavity in the original plane model be the same with those of simplified plane model. The basic concepts of these effective elastic constants are similar to those before-mentioned.

In the case of the test model, the effective elastic constants of the multicavity barrel are $E^* \approx 0.717 \cdot E_c$ and $\nu^* \approx \nu_c$.

In a similar manner, reinforcing steels provided in the structure are replaced by axisymmetric members.

(3) Evaluation of Local Loads

Suppose, the multicavity barrel subjected to local pressure only such as S/G cavity pressure, it should deform. Therefore, the modified axisymmetrical loads equivalent to the local loads shall be taken into account in the solid barrel wall.

The values of the equivalent axisymmetrical loads, $P_{E1}$ and $P_{E2}$ as shown in Fig.-5, are decided in a similar manner for the effective elastic constants. The values of $P_{E1}$ and $P_{E2}$ in the test model are

$$P_{E1} = -0.313 \cdot P_o \quad , \quad P_{E2} = 0.335 \cdot P_o \quad ,$$

where $P_{E1}$ is the radial pressure applied at the inner boundary to the region with effective elastic constants and $P_{E2}$ is the one at the outer boundary, and $P_o$ is the cavity pressure.

(4) Inelastic Responses of the Two Plane Models

The responses such as the pressure at concrete cracking and the position of cracks of the simplified plane model with axisymmetry are considered to coincide with those of the original plane model, because the elastic strain at critical position and the value of crack strain of concrete material are selected to be the same in both models. The effects of local cracks are neglected in the modified plane analysis, while those are taken into

account in the original plane analysis.

Fig.-6 shows their calculated results in radial displacements of both models. As shown in it, the result of the modified analysis is good agreement with that of the another.

Consequently, it is confirmed that the assumption used for this modified analysis are valid, not only elastic in elastic but also inelastic range.

3.2 Analytical Model with Three-Dimensional Solid Elements

Fig.-7 shows the model with three-dimensional solid elements for concrete crack analysis. This model is idealized so as to predict correctly the state of stress in the proto-type structure. The top head slab is replaced by the solid plate with the effective elastic constants as before-mentioned.

4. Calculated Results

The following articles present the calculated results using the two different procedures before-mentioned. In these figures, 2-D means the results of the modified two-dimensional analysis and 3-D means the results of the three-dimensional analysis.

The computation time to obtain the maximum load was 2 minutes in case of two-dimensional plane problem, and 24 minutes in case of axi-symmetrical problem with 39 load increments using IBM 360/195 computer. In case of three-dimensional problem with 14 load increments, the computation time was about 720 minutes using IBM 370/158 computer.

4.1 Elastic Response

(1) Load-Deflection Relationship

Typical load-deflection relationships are shown in Fig.-8. Both calculated results coincide well with the test results.

(2) Strain Distribution

Strain distributions at the equator of the barrel under 50 $kg/cm^2$ in internal pressure are shown in Fig.-9. The strain results obtained from the two-dimensional as well as the three-dimensional analysis compare favourably with the measured. In this figure, the values of 2-D are the modified values using the calculated results of original plane model representative of the multicavity barrel.

4.2 Inelastic Response

(1) Load-Deflection Relationship

Fig.-10 shows the load-deflection relationships for radial displacements at the equator of barrel, and Fig.-11 shows those for vertical displacements at the center of top head slab. The test model behaves elastically up to 70 $kg/cm^2$ in pressure, and it is distinct that the stiffness of the structure decrease gradually for the load beyond 135 $kg/cm^2$ in pressure. While, both calculated results of 2-D and 3-D are also similar to it.

The measured ultimate strength and the ultimate radial displacement at the equator are 238 $kg/cm^2$ and 3.3 mm respectively, while the calculated intensity due to 2-D analysis at the corresponding displacement is 235 $kg/cm^2$.

(2) Load-Strain Relationship

Typical load-strain relationships of winding wires are shown in Fig.-12, and load-strain relationships in concrete at the equator section are shown in Fig.-13. As shown in it, the calculated strain results, especially the ones of 3-D, coincide well with the measured.

(3) Concrete Crack Propagation

Fig.-14 shows concrete crack propagations due to 2-D analysis, and Figs.-15, 16, 17 show those at typical sections due to 3-D analysis. Table 2 presents the pressure values at concrete cracking.

The sequence of crack occurrence in the 2-D analysis is as follows: the first one is at the top corner of the inner side in barrel wall, the 2nd at the center of the outer surface of top head slab, the 3rd at the bottom corner of the inner side in barrel wall, the 4th at the equator of the inner surface on barrel wall, the 5th at the equator of the outer surface on barrel wall, and so on.

Such a sequence of crack occurrence and crack pattern are similar to those in the 3-D analysis and the measured.

Photos. 1 and 2 show the concrete crack distributions of the test model after experiment.

## 5. Conclusions

Consequently, the capabilities of the both analysis procedures are as follows:

(1) The Modified Two-Dimensional Analysis

This analysis procedure, using an analytical model idealized into axisymmetrical structure, is valid and reliable on the evaluation of inelastic as well as elastic response of a multicavity PCRV.

(2) The Three-Dimensional Analysis

This analysis procedure is able to predict correctly the inelastic as well as the elastic response of the structure up to the yielding state of steel material.

However, it seems to be uneconomical for the calculation of ultimate strength.

A method of inelastic analysis for three-dimensional problem up to the ultimate load capacity is being studied. In near future, the propriety of the method will be examined by comparison with the test results.

## 6. Acknowledgement

The experimental work of the 1/20th scale PCRV models described in this report was carried out based on the comments of Dr. A.J. Neylan, Dr. F.S. Ople and the others of General Atomic Company in U.S.A.. We express our gratitude to them.

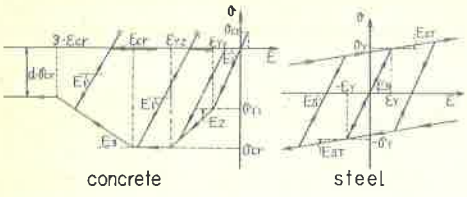


Fig.-1 Uniaxial stress-strain relationships of materials

Table-1 Material properties

1. Concrete

1) basic concrete (measured)

| | | |
|---|---|---|
| -0.455 | ton/cm² | compressive strength ($\sigma_B$) |
| -0.300 | " | yield strength ($\sigma_Y$) |
| 0.035 | " | tensile strength ($\sigma_T$) |
| 315 | " | young's modulus ($E_1$) |
| 150 | " | plastic modulus ($E_2$) |
| -0.003 | | ultimate strain ($\varepsilon_B$) |
| 0.167 | | poisson's ratio ($\nu$) |

assumed ratio of concrete properties at the other regions versus basic concrete

| region | $\sigma_B$ | $\sigma_Y$ | $\sigma_T$ | $E_1$ | $E_2$ | $\varepsilon_B$ | $\nu$ |
|---|---|---|---|---|---|---|---|
| 2) inner wall | 1.0 | 1.0 | 1.0 | 1.0 | 1.0 | 1.0 | 1.0 |
| 3) outer wall | 1.0 | 1.0 | 1.0 | 1.0 | 1.0 | 1.0 | 1.0 |
| 4) cavity | 0.717 | 0.717 | 0.717 | 0.717 | 0.717 | 1.0 | 1.0 |
| 5) stand pipe | 1.0 | 1.0 | 1.0 | 1.0 | 1.0 | 1.0 | 1.0 |
| 6) support | 0.83 | 0.75 | 0.75 | 0.75 | 0.75 | 1.0 | 1.0 |

2. Steel

hoop element

| | | |
|---|---|---|
| 17.0 | ton/cm² | $\sigma_Y$ |
| 2070 | " | $E_1$ |
| 20 | " | $E_2$ |

bar element

element No. 1-108

| | | |
|---|---|---|
| 12.77 | ton/cm² | $\sigma_Y$ |
| 2000 | " | $E_1$ |
| 20 | " | $E_2$ |

element No. 109-313

| | | |
|---|---|---|
| 2.4 | ton/cm² | $\sigma_Y$ |
| 2000 | " | $E_1$ |
| 20 | " | $E_2$ |

plate element (liner)

| | | |
|---|---|---|
| 2.8 | ton/cm² | $\sigma_Y$ |
| 2100 | " | $E_1$ |
| 21 | " | $E_2$ |
| 0.3 | | $\nu$ |

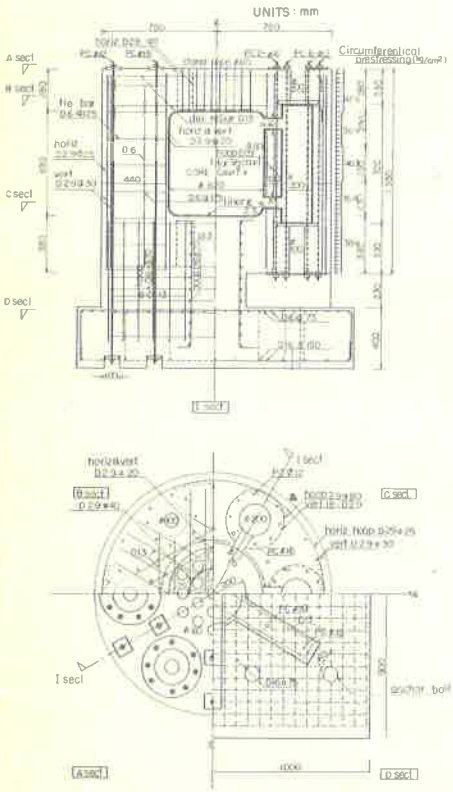


Fig.-2 1/20 PCRV test model

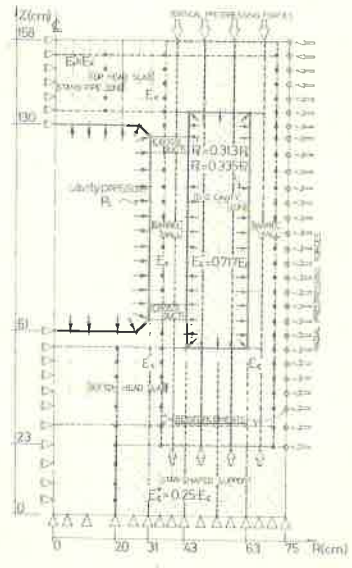


Fig.-3 Idealization of the axisymmetrical model (2-D)

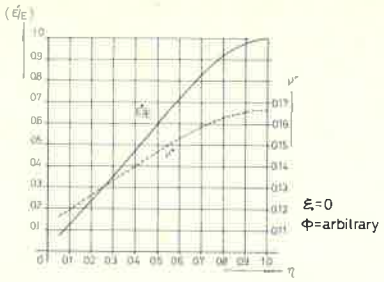


Fig.-4.1 Effective elastic constants without penetration liners

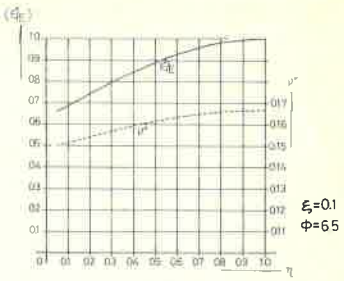


Fig.-4.2 Effective elastic constants with penetration liners

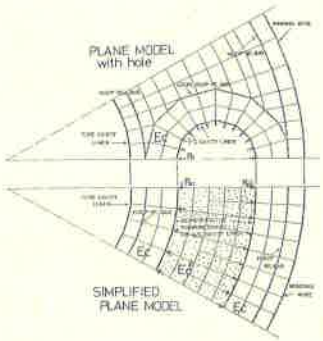


Fig.-5 Two different plane models for the barrel wall

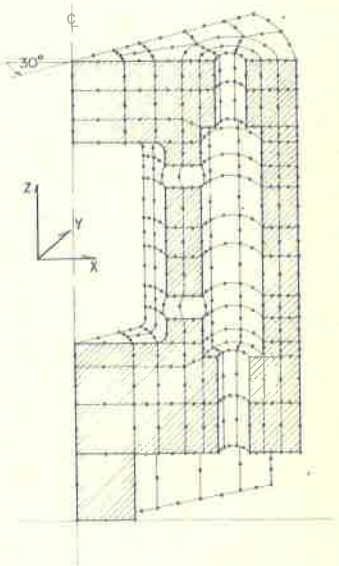


Fig.-7 Idealization of the finite element model (3-D)

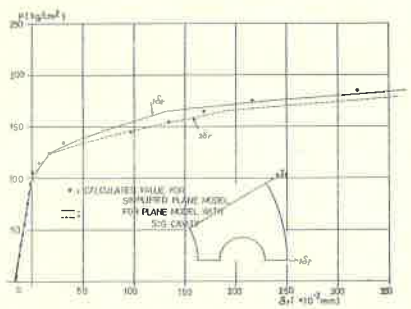

Fig.-6 Pressure-deflection curve in both plane analyses

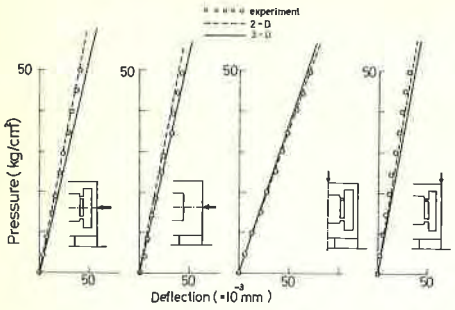


Fig.-8 Pressure-deflection curves in elastic range

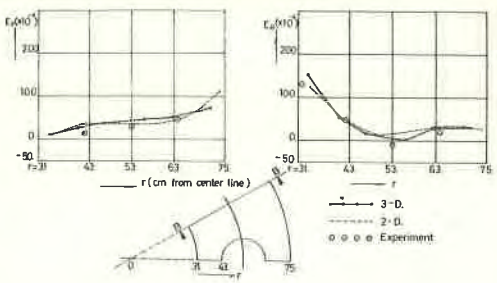


Fig.-9 Strain( $\varepsilon_z, \varepsilon_\theta$ ) distributions at section B-B on the equator; Pressure=50kg/cm$^2$

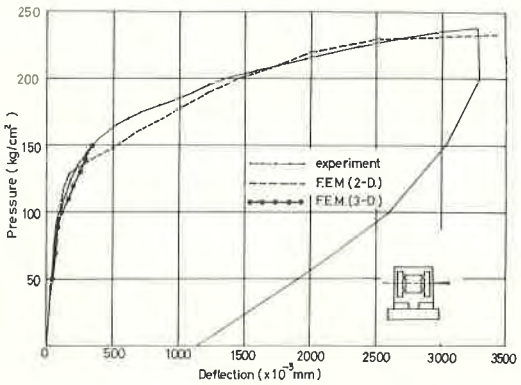


Fig.-10 Pressure-deflection curve at the equator

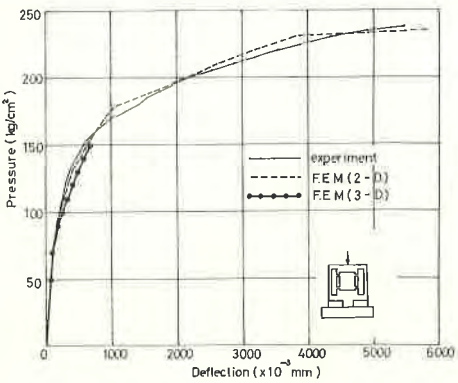


Fig.-11 Pressure-deflection curve at the center of the top head slab

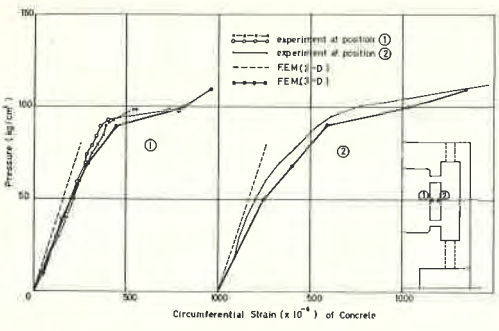


Fig.-12 Pressure-strain ($\varepsilon_\theta$) curve of the concrete at the inner wall of the equator

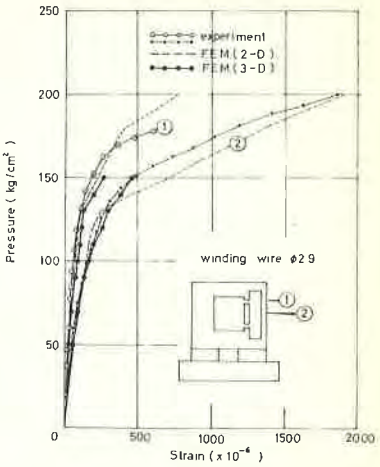


Fig.-13 Pressure-strain curve of the winding wire at position 1 and 2

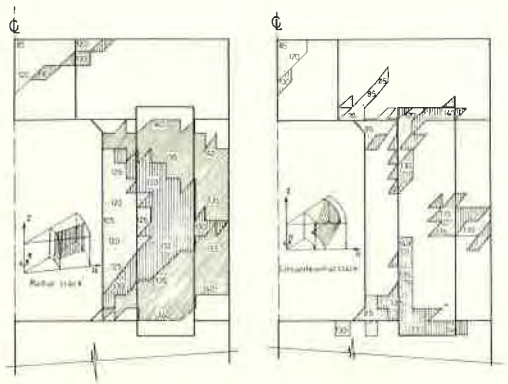

Fig.-4 Crack propagation obtained from the axisymmetrical analysis

Table-2 Comparison of the cracking pressure

| | location of the top head slab | pressure P(kg/cm²) | | |
|---|---|---|---|---|
| | | F.E.M.(3-D) | F.E.M.(2-D) | experiment |
| radial crack | at the center of the top head slab | 70 | 85 | 120 |
| | at the equator of the inner side | 90 | 105 | 100 |
| | at the equator of the outer side | 100 | 130 | 120 |
| circumferential crack | at the center of the top head slab | 110 | 85 | 120 |
| | at the top corner of the inner side | 70 | 70 | 90 |
| | at the bottom corner | 70 | 85 | 90-100 |
| | at the equator of the outer side | 120 | 115 | 120 |

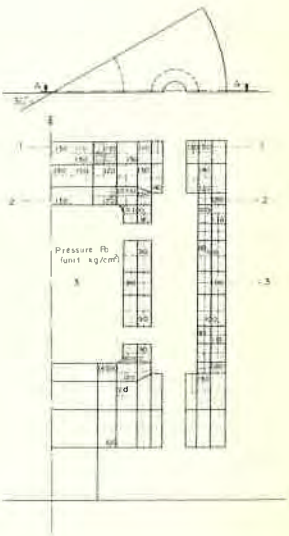

Fig.-15 Crack propagation at the vertical section A-A obtained from the 3-D F.E.M.

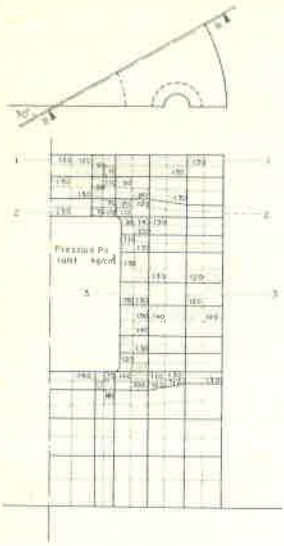

Fig.-16 Crack propagation at the vertical section B-B oftained from the 3-D F.E.M.

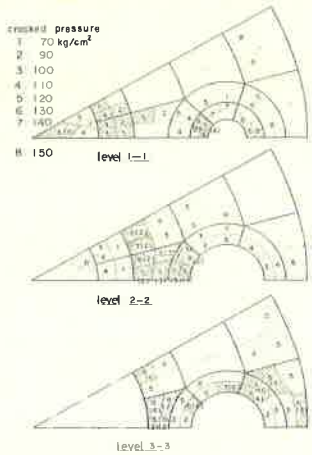


Fig.-17 Crack propagation at the three horizontal sections oftained from the 3-D F.E.M.

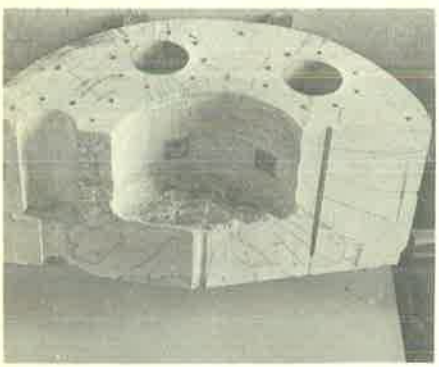

Photo.-1 Crack pattern of the concrete

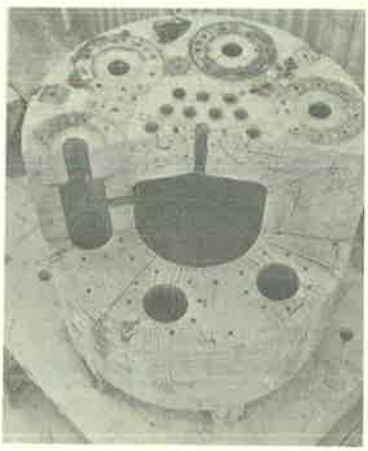

Photo.-2 Crack pattern of the concrete

References

(1) T. Slot, W.J. O'Donnel: "Effective Elastic Constants for Thick Perforated Plates with Square and Triangular Penetration Patterns", Journal of Eng. for Industry, Nov. ( '71 )

(2) T. Slot, J.P. Yalch: "Stress Analysis of Plane Perforated Structures by Point-Wise Matching of Boundary Conditions", Nuclear Eng. and Design, vol. 4 ( '66 )

(3) W.J. O'Donnell, B.F. Langer: "Design of Perforated Plates", Journal of Eng. for Industry, Aug. ( '62 )

(4) T. Takeda, et al.: "Pressure Tests of PCRV Models", 7th FIP/PCI International Conference, New York, May ( '74 )

(5) Y. Yamada, et al.: "Plastic Stress-Strain Matrix and Its Application for the Solution of Elastic-Plastic Problems by the Finite Element Method", International Journal of Mechanical Science, vol. 10, 1968, pp.343-354.

(6) B.M. Irons: "A Frontal Solution Program for Finite Element Analysis", International Journal of Numerical Methods in Engineering, vol. 2, 1970, pp.5-32.

(7) B Saugy, Th. Zimmermann and M. Hussain: "Three-dimensional Rupture Analysis of a Prestressed Concrete Pressure Vessel Including Creep Effects", Nuclear Eng. and Design 28 (1974) 97-120.